THE AEROSOL LAYER OF THE LOWER THERMOSPHERE: III. OBSERVATION IN ABSENCE OF THE MOON AND UNDER LARGE SUN'S ZENITH ANGLES

© 2025 A. N. Belyaev[a, *], S. Sh. Nikolaishvili[a, **], A. N. Omel'chenko[a, *], A. Yu. Repin[a, ****], M. A. Poluarshinov[b, *****], Yu. V. Smirnov[b, ******], A. V. Strakhov[c, *******], A. G. Batishchev[e, ********], V. I. Stasevich[c, **********], Yu. V. Platov[d, **********]**

[a] *Fedorov Institute of Applied Geophysics (IPG), Moscow, Russia*

[b] *S.P. Korolev Rocket and Space Corporation Energia (RKK Energia), Korolev, Russia*

[c] *Scientific Production Enterprise Robis (NPP Robis), Moscow, Russia*

[d] *Pushkov Institute of Terrestrial Magnetism, Ionosphere and Radio Wave Propagation (IZMIRAN), Russian Academy of Sciences, Moscow, Troitsk, Russia*

[e] *National Research Nuclear University Moscow Engineering Physical Institute (MEPhI), Moscow, Russia*

**e-mail: anb52@mail.ru*

***e-mail:* ser58ge@gmail.ru

****e-mail: alexom@mail.ru*

*****e-mail: repin_a_yu@mail.ru*

******e-mail: mikhail.poluarshinov@rsce.ru*

*******e-mail: yury.v.smirnov@rsce.ru*

********e-mail: lexand@robis.ru*

*********e-mail: alexey-batschev@mail.ru*

**********e-mail: walter@robis.ru*

***********e-mail: yplatov@mail.ru*

Received December 24, 2024

Revised February 03, 2025

Accepted April 14, 2025

Abstract. The results of the "Terminator" space experiment on board the International Space Station are given. Observations have been realized under limb geometry in the visual and near infrared ranges of the spectrum in absence of the Moon and under large Sun's zenith angles (> 145°). The treatment of the obtained digital photos has shown that our previous conception of the scattering mechanism of the observed emission layer to be faulty in absence of sun's backlight. In the present paper the emission of the observed layer is considered as thermal radiation of meteoric particles, preheated to 2000–3000 K on entering the atmosphere.

Keywords: *meteors, the upper mesosphere, the lower thermosphere, ablation, thermal radiation*

DOI: 10.31857/S00167940250410e9

1. INTRODUCTION

It is known that the Earth's atmosphere receives a large amount of "space dust" from space. According to various estimates, the intensity of this flow is in the range from 3 to 300 tons per day [Plane, 2012]. In the atmosphere, the flow of "cosmic dust" turns into a meteor stream. Due to collisions with air molecules, meteor particles are heated, melted, vaporized, crushed and atomized. As a result, at the heights of the upper mesosphere - lower thermosphere there is constantly present a stream of the smallest molten particles, whose masses lie in the range of $10^{-(10)}$-10^{-2} g [Carrillo-Sanchez et al., 2015], as well as aerosol particles generated by it, with sizes up to several hundred nanometers, formed as a result of coagulation processes of atoms initially vaporized from the surface of micrometeors [Plane, 2012].

Our previous articles [Belyaev et al., 2023, 2024] presented the results of photographic imaging of a layered atmospheric structure (SAS) located at the heights of the upper mesosphere-lower thermosphere. During the observations described in these articles, carried out within the framework of the Terminator space experiment, a large number of images of the SAS in the visible (540 nm) and near-infrared (700 and 830 nm) spectral ranges were obtained at different parts of the ISS orbit. Taking into account this circumstance, as well as the height of the registered luminous SAS, we assumed that the observed layered structure consists of aerosol, the appearance of which at the heights of the upper mesosphere - lower thermosphere is due to the ablation processes of meteoroids as they enter the dense layers of the atmosphere. It was assumed that the recorded SAS luminescence is caused by the scattering of sunlight on the meteor aerosol particles falling on them, either after reflection from the Moon's surface or after scattering in the atmosphere at the Earth's limb.

The present paper is devoted to testing this hypothesis. It will analyze photographs of the upper atmosphere taken from the ISS under conditions when there was no Moon in the sky and the zenith angle of the Sun was so large that the Earth's limb from the ISS was not viewable. It was expected that in these conditions optical registration of the presumed aerosol layer of meteoric origin would be impossible due to the lack of illumination. However, the images obtained refuted

these expectations. In all four spectral intervals in which the imaging was carried out, the images of the luminous SAS are distinguishable in the obtained photographs.

In the next section of the paper, we will describe in detail the conditions and parameters for imaging the luminous SAS from the ISS. The third and fourth sections will be devoted to the processing and analysis of the obtained digital images of the SAS. In the conclusion we will formulate the main conclusions and assumptions.

2. SHOOTING CONDITIONS AND PARAMETERS

The images were taken on June 20, 2023 from the ISS through the cabin porthole located on the starboard side of the Russian segment of the ISS using the equipment described earlier [Belyaev et al., 2023]. The atmospheric images presented here were obtained by cameras with interference filters for the wavelength ranges 540±5 nm, 700±5 nm, and 830±5 nm, with an exposure time of 1 s, without using the technology of merging the readings of neighboring pixels (binning). The atmospheric images taken by the fourth camera in the wavelength range 450±5 nm are not considered due to their very large noise.

Figure 1.

All eighteen photographs under consideration were taken at the maximum value of the Sun's zenith angle at the current rotation, i.e. under the conditions of maximum shading of the ISS and the photographed region of the atmosphere. Table 1 summarizes data on the geographic coordinates of the ISS, the position of the Sun and the Moon relative to the station at the moments of imaging. A similar table (see Table 2) summarizes data on the geographic coordinates of the photographed atmospheric regions with the corresponding zenith angles of the Sun and the Moon. Fig. 1 shows the geographical position of the ISS and the photographed areas of the SAS.

Table 1

Table 2

Figure 2.

3. IMAGE PROCESSING

Fig. 2 presents 3 typical for this observation session photographs of the atmosphere taken in three wavelength intervals at the moment when the ISS was at the point with geographic coordinates 35° S, 133° W (position No. 1 in Fig.). In each of these photographs there is an image

of the luminous SAS, despite the absence of illumination from the Moon and the Earth's limb. For the same reason, the Earth's surface, horizon, and limb cannot be seen in the photographs. At the same time, the image of the SAS is quite distinguishable. It is best visible in the wavelength range of 700±5 nm, slightly less contrasty in 830±5 nm and rather weakly in the visible range of 540±5 nm. Note that in the photograph of the atmosphere not shown here, taken with a camera with a filter for the wavelength range 450±5 nm, the presence of this luminous layer is also guessed.

Since all images of the luminous SAS in the Terminator experiment were obtained at the sensitivity limit of the recording equipment, the only way to obtain statistically significant data on the altitudinal course of the SAS brightness is to average over the entire ensemble of vertical photometric profiles present in the image. For this purpose, we used the technique of averaging digital atmospheric images described in our previous paper [Belyaev et al., 2024].

Figure 3.

The result of averaging the SAS image obtained in the 700±5 nm wavelength range at the moment when the ISS was at position No. 1 (see Fig. 1) is shown in Fig. 3. 3. The vertical profile presented in this figure should be interpreted as the averaged vertical profile of the atmospheric brightness measured in ADC units of the pixels of the photosensitive matrix. The vertical brightness profile presented in Fig. 3, the vertical brightness profile is a typical brightness profile of a spherical SAS observed in limbo geometry from Earth orbit. A characteristic feature of the vertical course of the brightness of the observed SAS is its sharp decline above the maximum level followed by a constant background value determined by contributions from zodiacal light, radiation from small stars, and hardware noise. Below the level of the maximum, the brightness of the observed SAS gradually decreases as it approaches the Earth's horizon. All the initial vertical brightness profiles analyzed in this paper have a similar shape.

Figure 4.

At the next stage of processing, the initial brightness profiles were reduced by the background value. As a result, a set of profiles was obtained, shown in Fig. 4, where the brightest are the profiles obtained by the camera with the 700±5 nm filter, and the dimmest are the profiles obtained in the visible wavelength range of 540±5 nm. However, if we consider the spectral efficiency of photon registration by the SONY ICX285 array (≈ 1 for λ= 540 nm, ≈ 0.7 for λ= 700 nm and ≈ 0.3 for λ= 830 nm), then the brightest CAC image would be the near-infrared image (λ= 830±5 nm), the image in the wavelength range λ= 700±5 nm would be the second brightest, and the visible image

(λ= 540±5 nm) would remain the third brightest. The corresponding CAC brightness profiles are shown in Fig. 5. We used these profiles to calculate the bulk luminosities of CAC in the wavelength intervals considered.

Figure 5.

The method of calculating the magnitude of the volume luminosity of a spherical SAS from its image obtained from an orbital station with limbo observation geometry is described in detail in [Gurvich et al., 2002] and used in our previous work [Belyaev et al., 2024]. The formal condition for the applicability of the transition from the vertical brightness profile of a spherical SAS to its bulk luminosity is the condition of constancy of the vertical luminosity course in the probed region having a horizontal extent of at least $2\sqrt{\Delta h R}$, where Δh is the thickness of the SAS and R is its radius [Gurvich et al., 2002]. Therefore, reconstructed from the brightness profiles presented in Fig. 5, the vertical course of the volume luminosity of the SAS is not the true, but some effective vertical profile forming the same brightness field for an observer on the ISS as the true distribution, which depends not only on the altitude, but also on the horizontal coordinate. Just such vertical profiles are shown in Fig. 6. We cannot judge from them the absolute value of the bulk luminosity, but we can speak about their relative contribution to the total luminosity of the observed SAS.

Figure 6.

4. ANALYSIS AND INTERPRETATION OF RESULTS

The images of the luminous SAS obtained in the absence of illumination from the Sun and the vertical profiles of the brightness and volumetric luminosity of the atmosphere calculated on their basis raise the question about the nature of the luminescence of the observed layered structure. Obviously, our previous version of the mechanism of the glow of this SAS [Belyaev et al., 2023, 2024] is incorrect, since the scattering of sunlight on aerosol particles of meteoric origin cannot explain the glow of the SAS at large zenith angles of the Sun (> 145°). At the same time, the registration of SAS simultaneously in 4 wavelength ranges allows us to consider this layered structure as an emission layer with a continuous emission spectrum in the wavelength range from 450 to 830 nm. A natural candidate for the role of the source of this spectrally continuous emission is, in our opinion, the flow of meteoroids entering the atmosphere, burning in it and thus radiating like any other heated body. It is this part of the meteoroid stream, it is proposed to consider as a source of spectrally continuous thermal radiation, registered in the "Terminator" CME.

Table 3.

In Table 3, the first three rows summarize the maximum values of the vertical profiles presented in Fig. 5. In the three lines below, the values of their pairwise relations and the corresponding values of the relations of the functions F_T(λ

$$F_T(\lambda) = \frac{\lambda^{-4}}{e^{\frac{hc}{\lambda k_B T}} - 1}, \quad (1)$$

calculated for selected values of the temperature *T of* a completely black body. Here λ is the wavelength of radiation, *h* is Planck's constant, *c* is the speed of light, k_B is Boltzmann's constant. Comparison of theoretical and real values of the ratios shows that the temperature of the observed CAC (at the height of its maximum brightness) is approximately equal to the temperature values given in the last row of this table.

The data presented in Table 3 indicate the predominance of thermal emission in the vicinity of the maximum brightness of SAS, despite the fact that in the spectral range of 830±5 nm there should be a contribution from the $P_{1)(1}$ and $P_2(1_)$lines of the OH(6-2$_)$band, and in the spectral intervals of 540±5 and 700±5 nm there may be weak spectrally unresolved molecular bands of other atmospheric gases. Nevertheless, as can be seen from Table 3, the ratio of the magnitudes of the brightness maxima of the different spectral ranges is consistent with the Planck distribution. Consequently, the main contribution to the SAS luminescence in the region of maximum brightness is given by the thermal emission of micrometeors whose temperature is close to the temperature values given in the last line of Table 3. At the same time, in upper and lower parts of the SAS (see Fig. 5), the ratio of brightnesses of different spectral ranges can significantly differ from the corresponding ratio in the vicinity of the maximum brightness of the SAS, which can be the result of changes in the temperature of micrometeors, as well as the presence of other atmospheric emissions.

In order to get an idea of the value of characteristic values of the thermal radiation intensity of a meteor stream entering the Earth's atmosphere, let us estimate the value of the spectral density of the zenith brightness $S_{(B)\ of}$ a model meteor stream at a wavelength λ= 700 nm, as well as the value of its zenith brightness *B* in the wavelength range 500-1000 nm. We will proceed from the following assumptions. Let a monodisperse meteor stream with a power *P*= 100 t/day enters the Earth's atmosphere. The mass of spherical meteor particles $m = 10^{-9}$ g, and their density ρ_m= 2 g/cm^3. Taking into account the above estimates of the temperature of the observed luminous SAS, we will assume that in the altitude range of 80-100 km, the temperature of meteoric particles will be

T= 2600 K. Thermal radiation of these particles will be considered as radiation of an absolute black body. Then the zenith spectral brightness $S_B(\lambda)$ of the meteor stream will be written in the following form:

$$S_B(\lambda) = \frac{2\pi c}{\lambda^4} \frac{\sigma \cdot \Delta z}{e^{\frac{hc}{\lambda k_Б T}} - 1} n, \quad (2)$$

where Δz = 20 km is the thickness of the radiating layer of the meteor stream, n is the volume concentration of particles in the meteor stream, σ = 3-10^{-10} m^2 is the surface area of a spherical meteor particle of mass 10^{-9} g. Assuming that the energy transferred to the meteor particle by oncoming air molecules is spent exclusively on thermal radiation, we estimate their velocity v by the following formula

$$v = 2\left(\frac{\pi k_c T^4}{\rho_a}\right)^{\frac{1}{3}}. \quad (3)$$

Here ρ_a= 3.4-10^{-6} kg/m^3 is the density of the atmosphere at an altitude of 90 km, k_c is the Stefan-Boltzmann constant. Estimating the velocity using formula (3) gives v= 18 km/s for meteoric particles with temperature T= 2600 K. The volume concentration of particles n in the considered meteoric stream is calculated from the ratio determining the rate of arrival of meteoric matter into the Earth's atmosphere

$$P = \pi n v m R_e^2 \quad (4)$$

where R_e= 6380 km is the radius of the Earth. Whence it follows that in the meteor stream with the power P= 100 t/day, the particle velocity v= 18 km/s the volume concentration of particles will be the value n= 5·10^{-7} particles/m^3. Substituting this value into formula (2), we obtain the value of the spectral density of the zenith brightness of the model meteor stream at wavelength λ= 700 nm equal to S_B= 1 Rl/nm. Integrating (2) from λ= 500 nm to λ= 1000 nm, we obtain the value of the integral zenith brightness *B of the* model meteoroid flux in this spectral range B= 577 Rl.

5. CONCLUSION

This paper is the final in a series of articles devoted to presenting preliminary results of the Terminator space experiment conducted in 2021-2024 on the ISS. In it, we abandoned the treatment of the observed luminous SAS as a light-scattering aerosol layer. In the present paper, we propose

to consider the luminosity of the observed SAS as thermal radiation from the flow of molten meteor particles entering the atmosphere. Accordingly, the observed luminous SAS is proposed to be interpreted as a layer of the atmosphere (80-100 km) in which the molten meteor particles flying through it, heated to a temperature of 2000-3000 degrees Celsius, emit with maximum intensity

In conclusion, we would like to recall the existence in middle atmosphere physics of the continuum problem - weak emission with a continuous spectrum, the mechanism of generation of which remains unexplored to date [Shefov et al., 2006; Semyonov et al., 2014a, b; McDade et al., 1986; Noll et al., 2012, 2024], while paying attention to the fact that the emission spectrum of meteor particles burning in the atmosphere is continuous, and the estimate of the brightness value of the considered model meteor stream in the visible and near-infrared spectral ranges (500-1000 nm) $B \approx 0.58$ kRL is not much less than the experimentally measured value of 2.7 kRL [Noll et al., 2024]

In order to formulate final conclusions about the nature and mechanism of the luminescence of the SAS observed by us and to answer the question about its possible connection with the continuum problem, it is necessary to continue the observations and construct a mathematical model, explaining and reproducing the quantitative characteristics of this atmospheric phenomenon.

REFERENCES

1. *Belyaev A.N., Nikolayshvili S.Sh., Omelchenko A.N., Repin A.Yu., Poluarshinov M.A., Smirnov Y.V., Strakhov A.V., Batischev A.G., Stasevich V.I., Platov Y.V.* Aerosol layer of the lower thermosphere: I. Observation against the background of the Earth's limb // Geomagnetism and Aeronomy. T. 63. № 4. C. 455-466. 2023. https://doi.org/10.31857/S0016794023600400

2. *Belyaev A.N., Nikolaishvili S.Sh., Omelchenko A.N., Repin A.Yu., Poluarshinov M.A., Smirnov Y.V., Strakhov A.V., Batischev A.G., Stasevich V.I., Platov Y.V.* Aerosol layer of the lower thermosphere: II. Observation at full Moon // Geomagnetism and Aeronomy. T. 64. № 5. C. 688-700. 2024. https://doi.org/10.31857/S0016794024050097

3. *Gurvich A.S., Vorobyov V.V., Savchenko S.A., Pakhomov A.I., Padalka G.I., Shefov N.N., Semenov A.I.* Night glow of the upper atmosphere in the range 420-530 nm according to measurements on the orbital station "Mir" // Geomagnetism and Aeronomy. T. 42. № 4. C. 541-546. 2002.

4. *Semenov A.I., Shefov N.N., Medvedeva I.V.* Empirical model of continuum emission variations in the upper atmosphere. 1. Intensity // Geomagnetism and Aeronomy. T. 54. № 4. C. 528-539. 2014a. https://doi.org/10.7868/S0016794014040154

5. *Semenov A.I., Shefov N.N., Medvedeva I.V.* Empirical model of continuum emission variations in the upper atmosphere. 2. Infrared Components // Geomagnetism and Aeronomy. T. 54. № 5. C. 701-712. 2014б. https://doi.org/10.7868/S0016794014050162

6. *Shefov N.N., Semenov A.I., Khomich V.Yu.* Radiation of the upper atmosphere - an indicator of its structure and dynamics. Moscow: GEOS, 740 p. 2006.

7. *Carrillo-Sanchez J.D., Plane J.M.C., Feng W., Nesvorny D., Janches D.* On the size and velocity distribution of cosmic dust particles entering the atmosphere // Geophys. Res. Lett. V. 42. N 15. P. 6518-6525. 2015. https://doi.org/10.1002/2015GL065149

8. *McDade I.C., Llewellyn E.J., Greer R.G.H., Murtagh D.P.* ETON 3: Altitude profile of the nightglow continuum at green and near infrared wavelengths // Planet. Space Sci. V. 34. N 9. P. 801-810. 1986. https://doi.org/10.1016/0032-0633(86)90076-0

9. *Noll S., Kausch W., Barden M., Jones A.M., Szyszka C., Kimeswenger S., Vinther J.* An atmospheric radiation model for Cerro Paranal. I. The optical spectral range // Astron. Astrophys. V. 543. ID A92. 2012. https://doi.org/10.1051/0004-6361/201219040

10. *Noll S., Plane J.M.C., Feng W., Kalogerakis K.S., Kausch W., Schmidt C., Bittner M., Kimeswenger S.* Structure, variability, and origin of the low-latitude nightglow continuum between 300 and 1800 nm: evidence for HO_2 emission in the near-infrared // Atmos. Chem. Phys. V. 24. N 2. P. 1143-1176. 2024. https://doi.org/10.5194/acp-24-1143-2024

11. *Plane J.M.* Cosmic dust in the Earth's atmosphere // Chem. Soc. Rev. V. 41. N 19. P. 6507-6518. 2012. https://doi.org/10.1039/C2CS35121

Table 1. Observation time, ISS coordinates, Sun and Moon positions

Twist	Shooting time is UTC, h:min:s	ISS coordinates		Sun		Moon	
		Longitude hail	Latitude hail	Zenith Angle hail	Azimuth hail	Zenith Angle hail	Azimuth hail
1	09:32:27	-133.0	-35.4	165.4	142.5	163.1	-116.5
2	11:05:17	-156.6	-35.4	165.6	143.6	162.4	-114.7
3	12:38:07	179.9	-35.4	165.8	144.8	161.3	-113.3
4	14:10:57	156.3	-35.3	166.0	145.9	160.6	-111.8
5	15:43:47	132.7	-35.3	166.1	147.1	159.5	-110.6
6	17:16:37	109.1	-35.3	166.3	148.3	158.7	-109.3

Table 2. Coordinates of the probed area and the corresponding zenith angles of the Sun and the Moon

№	Coordinates of the center of the probed area of the aerosol layer		Zenith angle of the Sun relative to the probed area, hail	Zenith angle of the Moon relative to the probed area hail
	Latitude, deg	Longitude hail		
1	-47.7	-114.9	147.2	158.9
2	-47.7	-138.5	147.4	158.9
3	-47.7	-162.1	147.6	158.8
4	-47.7	174.3	147.8	158.6
5	-47.6	150.8	148.0	158.3
6	-47.6	127.2	148.2	158.1

Table 3: Maximum CAC brightness values and their ratios

Shooting time UTC, h:min:s	09:32:27	11:05:17	12:38:07	14:10:57	15:43:47	17:16:37
$S_{\max}^{540}$ units. ADC	11.21	8.87	9.81	12.92	9.64	10.29
$S_{\max}^{700}$ units. ADC	38.26	33.97	27.48	33.51	27.34	29.29
$S_{\max}^{830}$ units. ADC	62.54	54.17	40.32	50.66	40.20	42.55
$S_{\max}^{830} : S_{\max}^{540} \big/ F_T(830) : F_T(540)$	5.58/5.64	6.11/6.24	4.11/4.19	3.92/3.92	4.17/4.19	4.13/4.19
$S_{\max}^{830} : S_{\max}^{700} \big/ F_T(830) : F_T(700)$	1.63/1.63	1.59/1.69	1.47/1.47	1.51/1.44	1.47/1.47	1.45/1.47
$S_{\max}^{700} : S_{\max}^{540} \big/ F_T(700) : F_T(540)$	3.41/3.45	3.83/3.69	2.80/2.84	2.59/2.72	2.84/2.84	2.85/1.84
T, K	2400	2340	2600	2650	2600	2600

Figure captions

Figure 1. Positions of the ISS and the photographed region of the atmosphere at the moments of imaging: 09:32:27 UTC (**1**), 11:05:17 UTC (**2**), 12:38:07 UTC (**3**), 14:10:57 UTC (**4**), 15:43:47 UTC (**5**), 17:16:37 UTC (**6**).

Figure 2. Photographs of the luminescent SAS in three bands (top at 540±5 nm, middle at 700±5 nm, and bottom at 830±5 nm).

Figure 3. High-altitude brightness profile of the luminescent CAC at a wavelength of 700 nm.

Figure 4. Vertical brightness profiles of the luminescent CAC. The discontinuous line is 540±5 nm, the thin continuous line is 830±5 nm, and the thick continuous line is 700±5 nm. The numbering of the graphs corresponds to the numbering in Fig. 1.

Figure 5. Vertical brightness profiles of the luminescent CAC corrected for the spectral sensitivity of the matrix. The discontinuous line is 540±5 nm, the thin continuous line is 830±5 nm, and the

thick continuous line is 700±5 nm. The numbering of the graphs corresponds to the numbering in Fig. 1.

Figure 6. Vertical profiles of the CAS bulk luminosity. The discontinuous line is 540±5 nm, the thin continuous line is 830±5 nm, and the thick continuous line is 700±5 nm. The numbering of the plots corresponds to the numbering in Fig. 1.

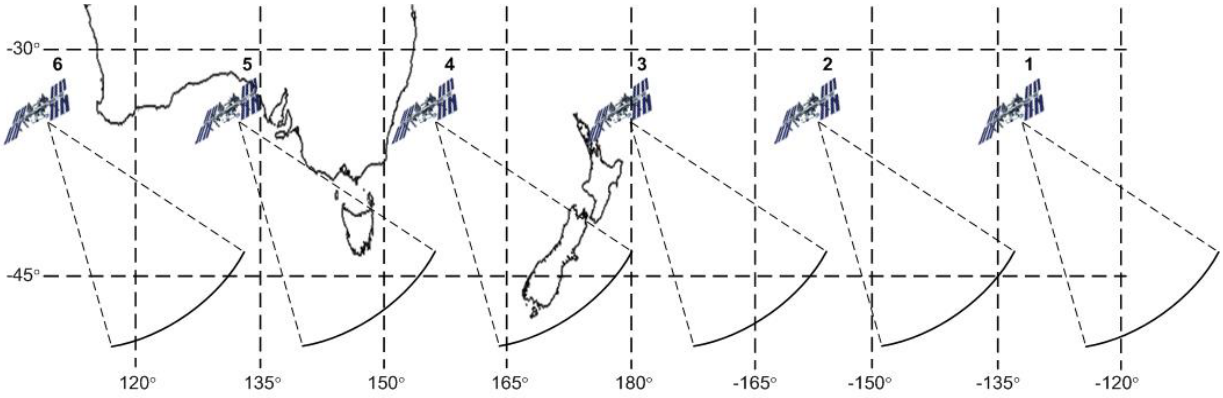

Figure 1.

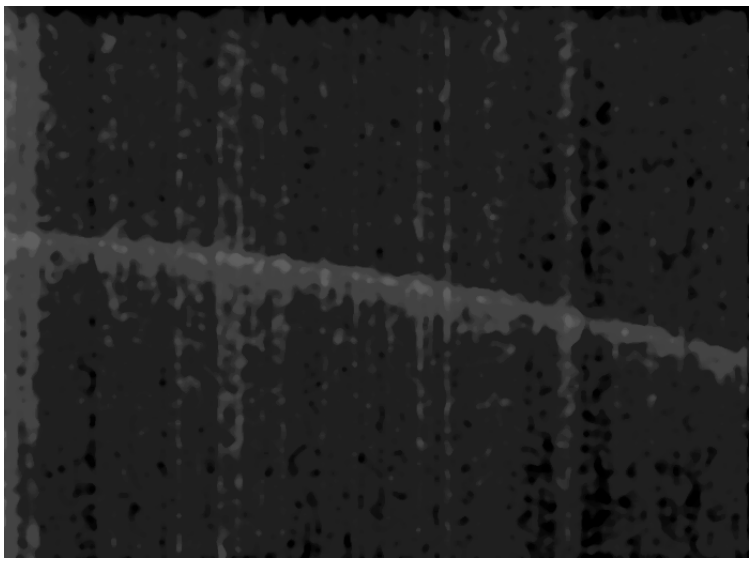

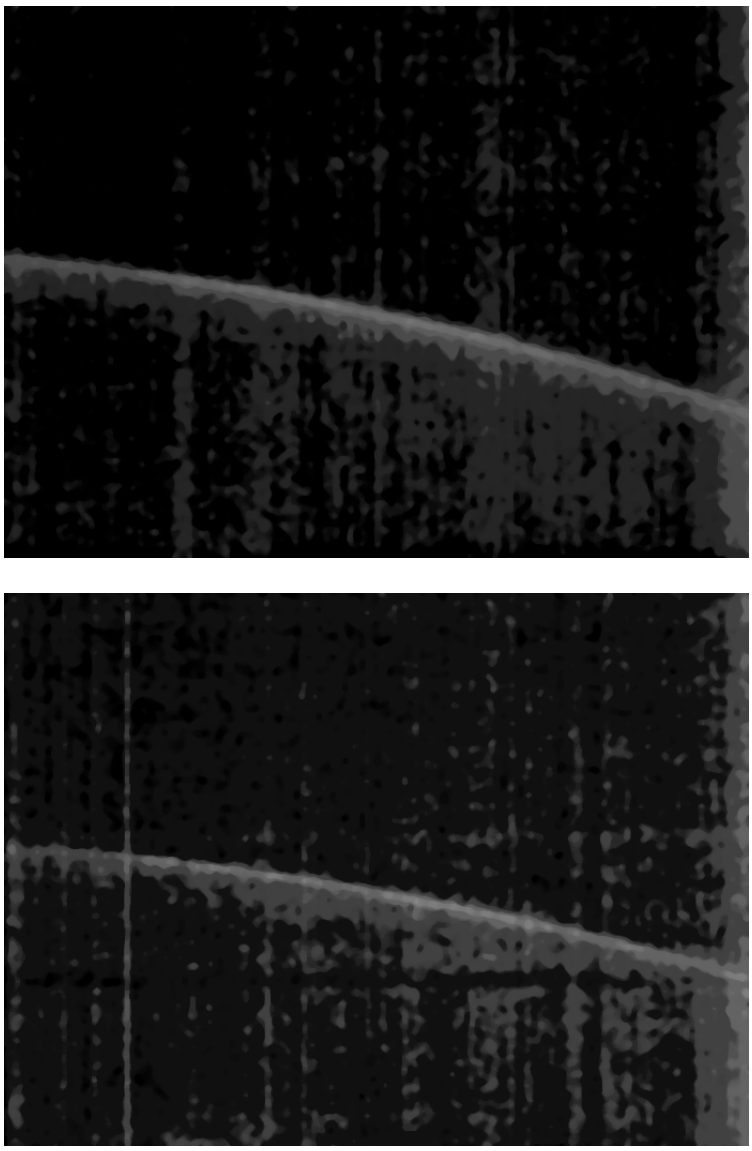

Figure 2.

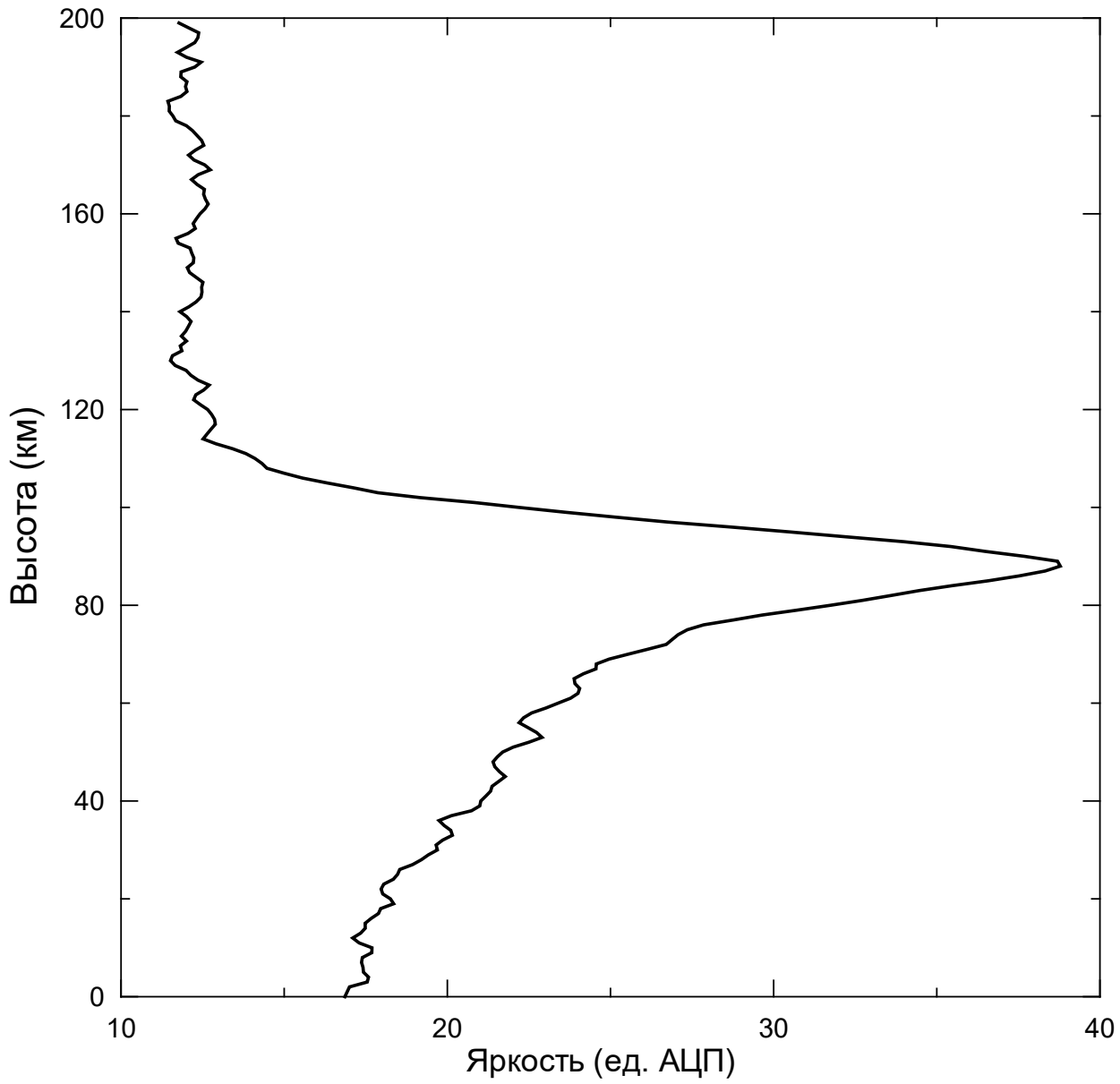

Figure 3.

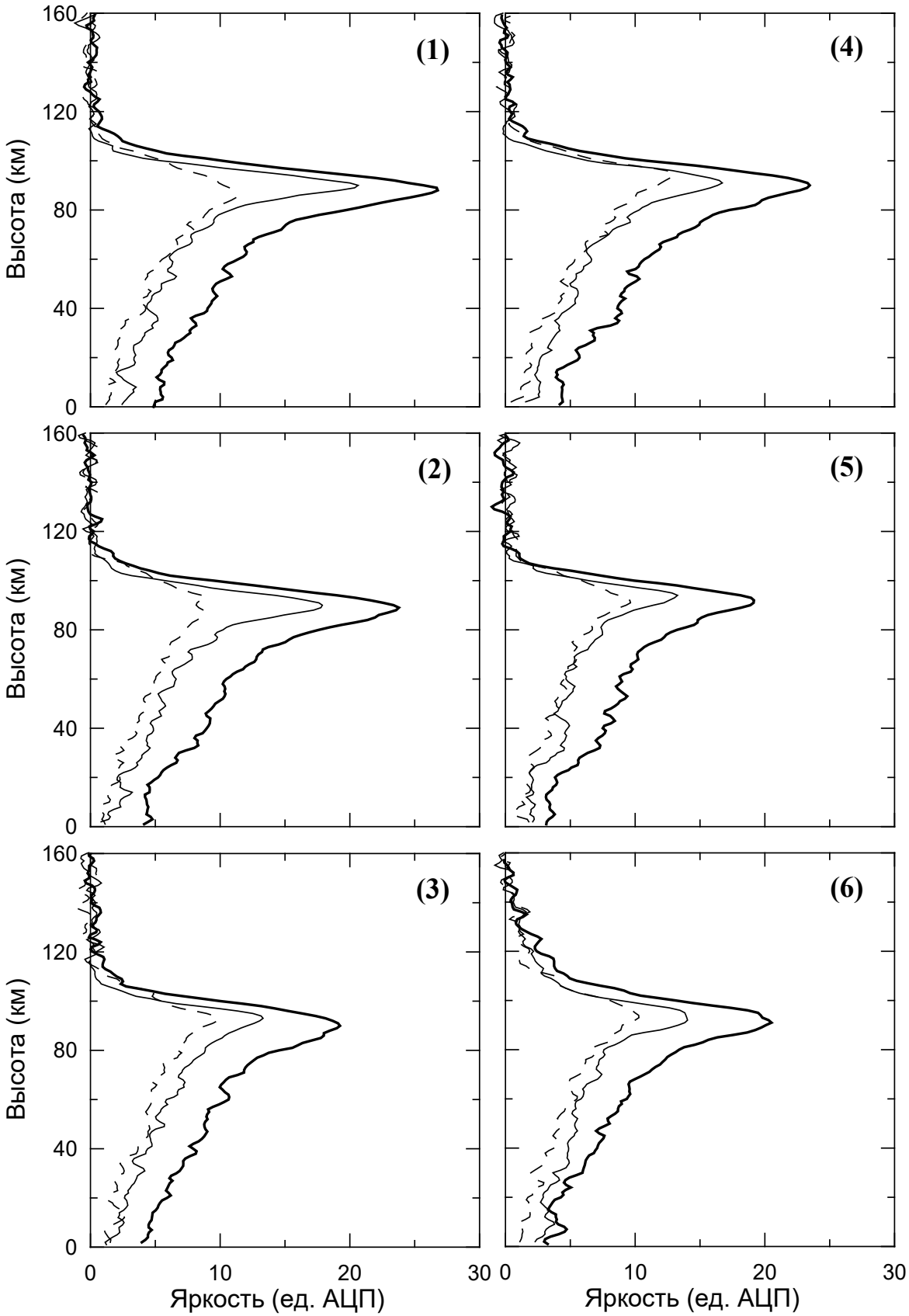

Figure 4.

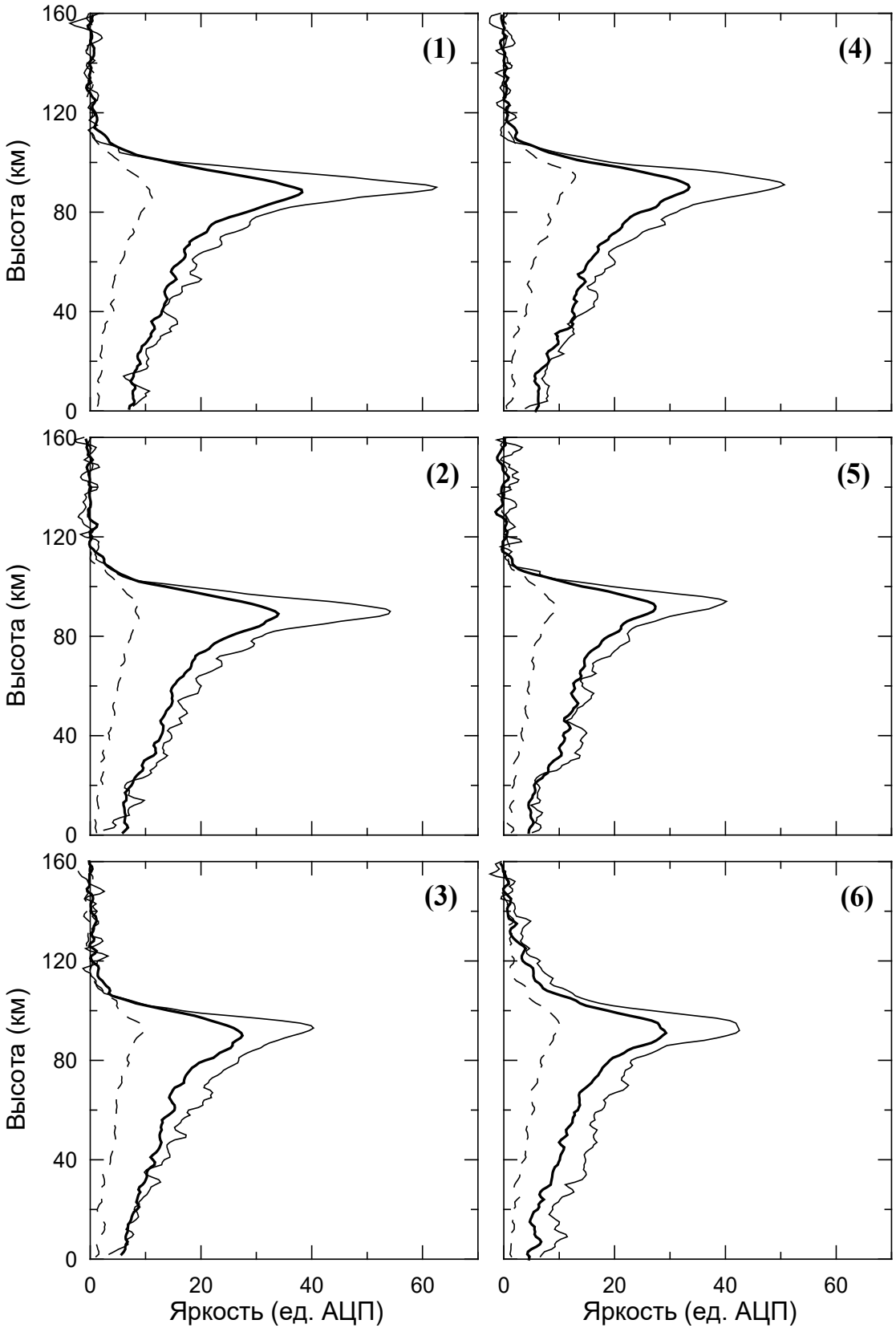

Figure 5.

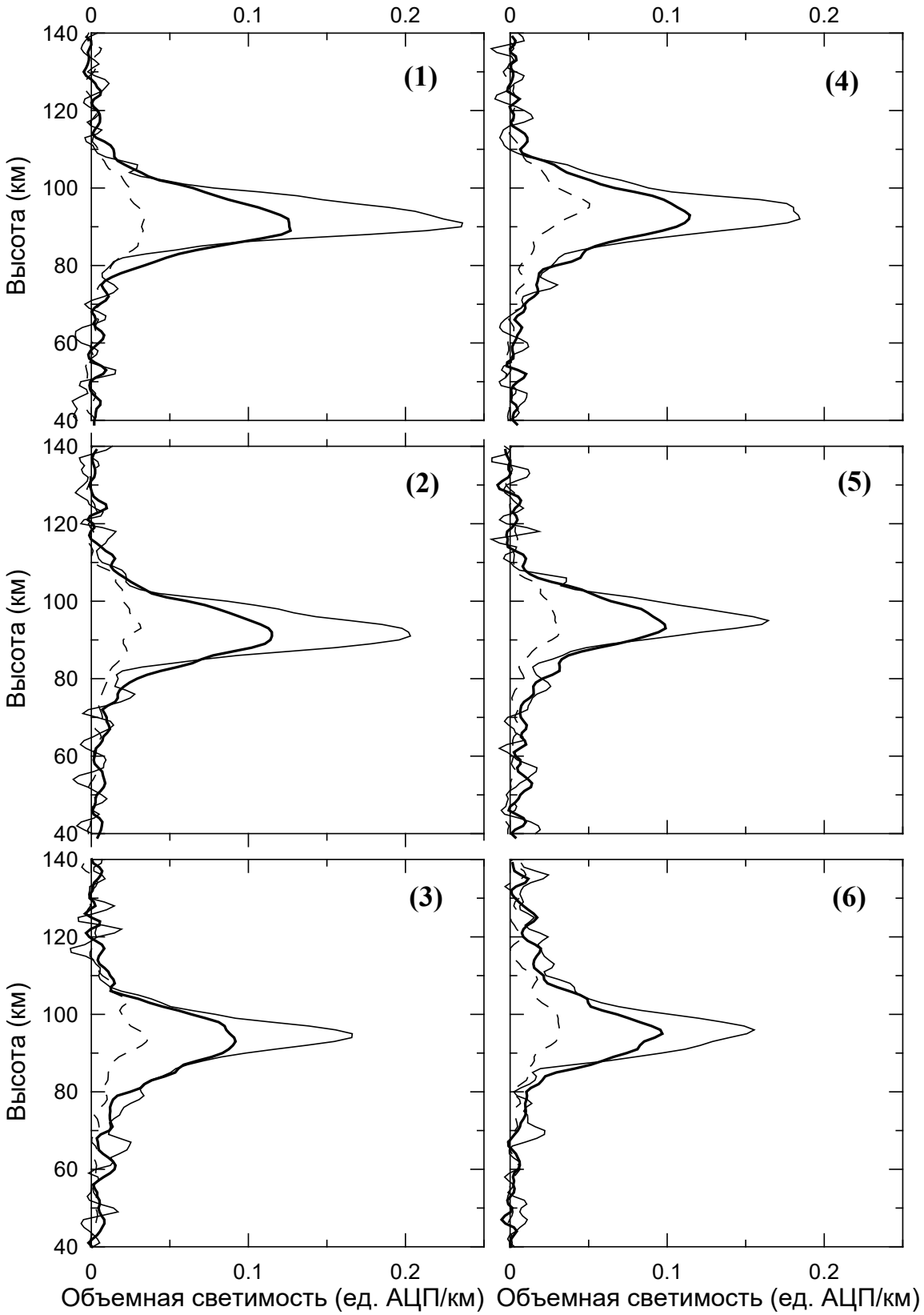
(1)
(2)
(3)
(4)
(5)
(6)
Высота (км)
Объемная светимость (ед. АЦП/км)
0
0.1
0.2
40
60
80
100
120
140

Figure 6